Multiple in-plane spin reorientation transitions in Fe/CoO bilayers grown on vicinal MgO(001)

Q. Li, T. Gu, J. Zhu, Z. Ding, J. X. Li, J. H. Liang, Y. M. Luo, Z. Hu, C. Y. Hua, H.-J. Lin, T. W. Pi, C. Won, and Y. Z. Wu

Phys. Rev. B **91**, 104424 — Published 25 March 2015

DOI: 10.1103/PhysRevB.91.104424

Multiple in-plane spin reorientation transitions in Fe/CoO bilayers grown on vicinal MgO(001)

Q. Li[1], T. Gu[1], J. Zhu[1], Z. Ding[1], J. X. Li[1], J. H. Liang[1], Y. M. Luo[1], Z. Hu[2], C. Y. Hua[2,3], H.-J. Lin[3], T. W. Pi[3], C. Won[4] and Y. Z. Wu[1*]

[1] Department of Physics, State Key Laboratory of Surface Physics and Collaborative Innovation Center of Advanced Microstructures, Fudan University, Shanghai 200433, China

[2] Max-Planck-Institut für Chemische Physik fester Stoffe, Nöthnitzer Str. 40, 01187 Dresden, Germany

[3] National Synchrotron Radiation Research Center, Hsinchu 30076, Taiwan, Republic of China

[4] Department of Physics, Kyung Hee University, Seoul 130-701, Republic of Korea China

ABSTRACT

Step-induced antiferromagnetic (AFM) uniaxial anisotropy and its effects on the exchange coupling have been systematically investigated in the epitaxial Fe/CoO bilayers on MgO(001) vicinal surface. X-ray magnetic linear dichroism measurements proved that the atomic steps induced a strong in-plane AFM uniaxial anisotropy in the CoO film. We found that the thermal activation induced in-plane 90-degree switching of CoO AFM in-plane spins. The competition among the step-induced AFM anisotropy, the interface exchange coupling and thermal activation generate novel multiple in-plane spin reorientation transition of the Fe magnetization, which can further provide new insights on the exchange coupling in FM/AFM systems.

I. INTRODUCTION

Antiferromagnetic (AFM) materials, being one of the fundamental systems with magnetic ordering, have been widely used in advanced magnetic storage and sensor devices [1,2], utilizing the exchange coupling effect in ferromagnetic (FM)/AFM bilayers. Recently, significant effort has been made to increase the application potential of AFM materials in so-called antiferromagnetic spintronics [3,4,5,6,7,8], where ferromagnetic electrodes are replaced by AFM ones. The performance of AFM spintronics is certainly related to the spin configurations of the AFM materials, making it crucial to be able to independently manipulate the AFM spin orientation as well as the AFM magnetic anisotropy of these materials beyond the exchange coupling effect at the AFM/FM interface.

The most promising method for tuning the anisotropy of an AFM thin film is to either induce lattice distortions in multiferroic systems or by growing the AFM thin film on a lattice-mismatched substrate. Multiferroics research [9] relies on the coupling of ferroelectric and magnetic polarization vectors, which is usually not strong enough. Lattice mismatching can provide a fine method to tune the AFM strain and modify the magneto-crystalline anisotropy of the AFM film [10-13]. As a good example, the AFM spins in a NiO film prefer the in-plane direction if grown on Ag(001) with compressed strain, but align along the out-of-plane direction when grown on MgO(001) with tensile strain [10]. The AFM spin orientation of CoO films grown on MgO(001) and MnO(001) can also be tuned either in-plane or out-of-plane by varying the film strain [11]. Moreover, AFM spin-reorientation transitions (SRTs) were demonstrated in NiO/MgO/Ag(001) [12] and CoO/MnO/MgO(001) [13] systems by continuously modifying the strain in the AFM film, and the different AFM spin orientations could induce significantly different exchange coupling effects.

Since most magnetoelectronic devices and antiferromagnetic spintronics devices are based on a spin-valve geometry, it is more desirable to control the in-plane antiferromagnetic spin direction. For NiO films grown on Ag(001) vicinal surfaces, the atomic steps could induce the in-plane uniaxial AFM anisotropy, and the NiO spins could be aligned either along or perpendicular to the steps direction depending

on the growth conditions [14]. The perpendicular coupling between Fe and NiO spins was proven by independently measuring the properties of Fe and NiO layers [15,16]. It is still unclear whether such a method to tune the in-plane AFM anisotropy via atomic steps could be adapted to other AFM systems. Moreover, it remains a question whether AFM spin orientation could be tuned under the influence of step-induced AFM anisotropy and the interfacial exchange coupling in FM/AFM bilayer, which may provide new insights into the exchange coupling effect between FM and AFM spins.

CoO was considered as a model system to study the exchange coupling effect in FM/AFM systems, because of its easily accessible Néel temperature ($T_N \sim 290$ K), which is close to room temperature (RT) [17,18], and the high-quality epitaxial growth of CoO films [19,20]. Moreover, the AFM properties of CoO films can be measured directly by the X-ray magnetic linear dichroism (XMLD) effect [11,13,19,21,22]. AFM spins in a CoO film grown on a MgO(001) flat surface prefer an in-plane direction with a strong four-fold anisotropy and the easy axis (EA) along the CoO<110> direction [23]. Because of spin-flopping coupling [24,25], field cooling in a Fe/CoO/MgO(001) system can induce a strong uniaxial anisotropy in the Fe film with the EA along the CoO<110> direction, which is close to the direction of the cooling field (H_{FC}), and with CoO AFM spins aligned perpendicular to H_{FC} [26].

In this paper, we report on the step-induced AFM anisotropy in CoO films grown on vicinal MgO(001) surfaces, and its effect on the exchange coupling in the Fe/CoO bilayer. By exploiting the XMLD effect, we found that the atomic steps induced an in-plane uniaxial AFM anisotropy in the CoO film grown on a MgO(001) vicinal surface with the steps parallel to the <110> direction. The exchange coupling effect in the Fe/CoO bilayers was studied through magneto-optic Kerr effect (MOKE) measurements. We found that the anisotropy in the Fe film induced by the exchange-coupling strongly depended on the orientation of H_{FC}. For an H_{FC} that points in a direction perpendicular to the steps, one in-plane SRT of Fe moments was found around the T_N of the CoO film. However, for an H_{FC} direction parallel to the steps, we found two temperature-driven SRTs, and three CoO-thickness-driven SRTs

at low temperatures, which have never been addressed before. These results point out the existence of thermally driven 90°-switching of CoO AFM spins. Hence, the competition among exchange coupling, AFM in-plane anisotropy, and thermal activation could generate new phenomena in FM/AFM systems.

II. EXPERIMENTS

The Fe/CoO/vicinal MgO(001) thin films were prepared by molecular beam epitaxy (MBE) in an ultra-high vacuum (UHV) chamber at a base pressure of 2×10^{-10} Torr. Vicinal MgO(001) (7° vicinal angle with steps parallel to the <110> direction) was used as the substrate. The commercial MgO substrates were first annealed at 600°C for 30 min in the UHV chamber, followed by a 10-nm-thick MgO seed layer growth at 500°C via e-beam evaporation. The sharp reflection high-energy electron diffraction (RHEED) patterns with electrons along the step direction demonstrated the smooth vicinal MgO(001) surface. The CoO layer was prepared by the reactive deposition of Co at an oxygen pressure of 5×10^{-7} Torr at RT, and this method has been proven to create smooth CoO film surfaces [13,26], which can be confirmed by RHEED patterns. To study the thickness-dependent properties, the CoO film can be grown with a wedged shape by moving the substrate behind a knife-edge shutter along the CoO <110> direction. In order to study the exchange coupling between the AFM CoO layer and the FM Fe layer, an Fe film was then grown by MBE at RT. In-situ RHEED patterns revealed a good epitaxy of both CoO and Fe on the MgO(001) substrates with an epitaxial relation specified as $Fe[100] \| CoO[110] \| \mathrm{MgO}[110]$ [13,26]. Finally, the sample was capped by a 3 nm MgO layer, which was used as a protective layer for MOKE measurements. For the samples used in the XMLD measurements, a 2 nm Au layer was capped on top of the CoO layer to avoid the charging effect. Film growth rates were determined using a calibrated quartz thickness monitor.

XMLD measurements were performed at the bending magnet Beamline 08B of the National Synchrotron Radiation Research Center (NSRRC). As shown in Fig. 1(a), a normal-incident X-ray with the polarization fixed along the horizontal direction was

used, and the XMLD effect was determined by changing the azimuthal angle (ϕ), which is defined as the angle between the X-ray polarization and the steps direction. The X-ray absorption spectrum (XAS) of the Co^{2+} L_3 edge was recorded in total electron yield mode by measuring the sample current. The sample temperature could be adjusted in the range given by 78–430 K with a precision of ~0.1 K.

The magnetic properties of the films were determined by MOKE measurements using a laser diode with a wavelength of 670 nm. By taking advantage of the small laser beam size (below 0.2 mm) in the MOKE measurements, we were able to systematically perform thickness-dependent studies on the same wedge-shaped sample. It was possible to rotate the magnetic field in the sample plane, enabling us to change the field cooling direction without changing the sample orientation. The sample temperature for the MOKE measurements could be adjusted in the range given by 80–330 K with a precision of ~0.1 K.

III. RESULTS AND DISCUSSION

XMLD measurements have proven that AFM CoO spins align along the film plane for CoO films grown on MgO(001) surfaces [11,13,19,21]. Fig. 1(b) shows the typical XAS of the Co^{2+} L_3 edge at normal incidence with the X-ray polarization parallel to the steps ($\phi = 0^o$) and perpendicular to the steps ($\phi = 90^o$) at T = 78 K, thereby clearly showing the existence of the X-ray linear dichroism (XLD) effect. The intensity of the first peak located at hν ~ 777 eV is lower for $\phi = 0^o$ than for $\phi = 90^o$. The XLD effect at the Co^{2+} L_3 edge can generally be attributed to the AFM ordering and the crystal-field effect [27,28]. While the AFM contribution vanishes above T_N, the crystal-field contribution still persists at high temperatures. Fig. 1(c) shows the absence of the XLD effect at 360 K, indicating that the observed Co^{2+} L_3-edge XLD effect obtained at normal incidence is solely because of its magnetic origin. We also systematically studied the XAS as a function of ϕ by azimuthally

rotating the sample (Fig. 1(c)). The L_3 ratio (R_{L_3}), which is defined as the ratio of the XAS intensities at 777 eV and 779.6 eV [marked as I_1 and I_2 in Fig. 1(b), respectively], was used to quantify the XMLD effect. Fig. 1(d) shows the ϕ -dependent R_{L_3} values for both 78 K and 360 K. It is clear that R_{L_3} at 78 K presents a two-fold symmetry with a maximum when $\vec{E} \perp steps$ and a minimum when $\vec{E} \parallel steps$. However, at 360 K, R_{L_3} shows an isotropic behavior. In Fig. 1(e), the L_3 ratio difference ΔR_{L_3} ($\Delta R_{L_3} = R_{L_3}(0^o) - R_{L_3}(90^o)$) decreases with increasing temperature and drops to zero around the T_N of the CoO film, further confirming the magnetic origin of the observed XLD effect in this film.

The easy axis of in-plane uniaxial anisotropy in AFM CoO film is along the step direction, which can be determined by the XMLD effects at the Co^{2+} L_3 edge. Van Laan *et al.* already pointed out that the XMLD effect at the Co $L_{2,3}$ edge exhibits a strong dependence on the relative orientation between the X-ray polarization, the AFM spin axis, and the crystalline axis [22]. For the CoO spins $\vec{\vec{S}}_{CoO}$ along the <100> direction, i.e. $\vec{\vec{S}}_{CoO} \parallel <100>$, the first peak around 777 eV has a higher intensity when $\vec{E} \parallel \vec{\vec{S}}_{CoO}$ than when $\vec{E} \perp \vec{\vec{S}}_{CoO}$, but the fourth peak around 779.6 eV has a lower intensity when $\vec{E} \parallel \vec{\vec{S}}_{CoO}$. Hence, the L_3 ratio $R_{L_3}(\vec{E} \parallel \vec{\vec{S}}_{CoO})$ should be larger than $R_{L_3}(\vec{E} \perp \vec{\vec{S}}_{CoO})$. However, if $\vec{\vec{S}}_{CoO}$ points along the <110> direction, the situation is reversed, and $R_{L_3}(\vec{E} \parallel \vec{\vec{S}}_{CoO})$ should be smaller than $R_{L_3}(\vec{E} \perp \vec{\vec{S}}_{CoO})$. The results of the XMLD measurements displayed in Fig. 1(d) clearly show a two-fold symmetry with the symmetric axis along the step direction. Hence, the CoO AFM spins should be either parallel or perpendicular to the step directions, being parallel to the <110> axis. The measured R_{L_3} is always smaller when $\vec{E} \parallel steps$ than when $\vec{E} \perp steps$, which indicates that $\vec{\vec{S}}_{CoO}$ should be parallel to the step direction. Therefore, our XMLD results prove that the atomic steps on a MgO(001)

vicinal surface can induce an in-plane uniaxial AFM anisotropy in the CoO film, with the EA along the steps direction ($\vec{S}_{CoO} \parallel steps$). We also obtained CoO-thickness dependent XMLD measurements on a wedge-shaped CoO film, and found a similar XMLD effect up to a thickness of 14 nm. For a NiO film grown on a Ag(001) vicinal surface at a certain growth temperature, an in-plane NiO AFM SRT was observed due to the NiO lattice relaxation [29], which does not exist in a CoO film on a MgO(001) vicinal surface.

The effect of the in-plane uniaxial AFM anisotropy on the exchange coupling at the FM/AFM interface was further investigated with hysteresis analysis in a Fe(18 nm)/CoO(4 nm) bilayer grown on a MgO(001) vicinal surface, which confirms the results from XMLD data. It should be noted that the deposition of FM layer may influence the AFM domain structure and the deposition of Co layer on NiO(001) surface could induce a spin reorientation of Ni interface moment from the <112> directions to the <110> directions [30,31]. However, in our Fe/CoO bilayer system, both the Fe moments and the CoO moments are lying in the film plane, thus we believe that the step-induced in-plane AFM uniaxial anisotropy still remains after the Fe deposition, which can be confirmed by the following results of MOKE measurement. Fig. 2(a) and 2(b) show the typical magnetic hysteresis loops of a Fe/CoO bilayer obtained at 330 K and 80 K, respectively. At 330 K, the Fe/CoO system shows a rectangular EA loop when $H \parallel steps$ and a double-split hard-axis (HA) loop when $H \perp steps$, indicating an in-plane uniaxial anisotropy of the Fe film with $EA \parallel steps$, which is induced by the atomic steps [32]. However, as shown in Fig. 2(b), while the sample is cooled down to 80 K, the EA of the Fe film is switched to the direction perpendicular to the steps. The double-split HA loops can be characterized by the shift field Hs, defined by the offset of the minor loop, which is proportional to the strength of the in-plane uniaxial anisotropy [32,33,34]. Fig. 2(c) shows the temperature-dependent Hs, which decreases with increasing temperature and saturates at a negative value at T ~ 300 K. Here we define a positive value of Hs

for the HA loop with $H \parallel steps$, and a negative value of Hs for the HA loop with $H \perp steps$, Thus sign-change of Hs is due to the 90°-switching of the Fe EA. The temperature-dependent Hs measured for an 18-nm-thick Fe film on a MgO vicinal surface is plotted in the inset of Fig. 2(c) for comparative purposes, and exhibits only slight changes with varying temperatures. Hence, the transition of Hs in the Fe/CoO bilayer should be attributed to the AFM order of the CoO film. At a temperature below the T_N of CoO, the XMLD measurement results in Fig. 1 show that because of the step-induced AFM anisotropy, the CoO spins align along the steps direction. Therefore, the spin-flop coupling [24,25] between the FM Fe spins and the AFM CoO spins induces an uniaxial anisotropy of the Fe film with $EA \perp \vec{S}_{CoO}$ [26]. The temperature-dependent coercivity Hc of the EA loops is plotted in Fig. 2(d), which also shows a clear transition at T ~ 300 K.

Interestingly, we found that the orientation of cooling field strongly affects magnetic properties of Fe/CoO bilayers on MgO(001) vicinal surface. Temperature-dependent loops were measured after cooling down from 330K to 80K using $H_{FC} = 1\,\mathrm{kOe}$. The in-plane H_{FC} was applied either parallel or perpendicular to the steps, and the sample orientation was adjusted with either $H \perp steps$ or $H \parallel steps$. Fig. 3 shows typical hysteresis loops of a Fe(18 nm)/CoO(4 nm) bilayer measured at various temperatures employing four different geometries as indicated by the schematic drawings above the loops. In our measurement, the exchange bias field at low temperature is usually only a few Oe which is much smaller than the anisotropy field, and such weak exchange bias can be attributed to the compensated spin structure at the CoO(001) surface [13,35].

When $H_{FC} \perp steps$, there is an obvious in-plane SRT of the Fe layer in which the EA switched from the direction perpendicular to the direction parallel to the steps, as shown in Fig. 3(a) and Fig. 3(b), exhibiting a behavior that is similar to the case of zero field-cooling displayed in Fig. 2. When $H_{FC} \perp steps$, the Fe magnetization

M_{Fe} was aligned perpendicular to the steps during the cooling process. In this case, the spin-flop coupling aligned $\vec{S}_{CoO}$ parallel to the steps and induced an uniaxial anisotropy of the Fe film with $EA \perp steps$ at low temperatures ($T < T_N$).

For $H_{FC} \parallel steps$, two temperature-dependent SRTs can be observed, as shown in Fig. 3(c) and 3(d). The EA of the Fe film first switches from $EA \parallel steps$ to $EA \perp steps$ at lower temperature, and switches back to the step direction at a temperature of ~ 300 K. The second SRT can be explained by the establishment of a CoO AFM order when $EA \parallel steps$, similar to the case where $H_{FC} \perp steps$. The first SRT observed at a lower temperature can be attributed to the CoO AFM SRT that changes from a direction perpendicular to a direction parallel to the steps. When the Fe/CoO bilayer is cooled down with $H_{FC} \parallel steps$, the spin-flop coupling aligns the CoO AFM spin in the direction perpendicular to the steps, i.e. $\vec{S}_{CoO} \perp steps$. For the system in which the steps are parallel to the CoO<110> direction, both the directions parallel and perpendicular to the steps are the EAs of the CoO in-plane four-fold anisotropy [23,26]. Hence, in this case the CoO spins can still remain oriented perpendicular to the steps, although this is the HA of the step-induced uniaxial anisotropy. However, the CoO spins can only stay oriented along this metastable state at low temperatures, switching back to their ground state with $\vec{S}_{CoO} \parallel steps$ due to thermal activation at higher temperatures.

It should be noted that the first SRT shows different transition temperatures for different field orientations relative to the steps (Fig. 3(c) and 3(d)). This SRT happens at ~ 208 K for $H \parallel steps$, but at ~ 115 K for $H \perp steps$. Such a difference in transition temperature reflects the influence of the exchange coupling at the Fe/CoO interface. Owing to the spin-flop coupling effect at the Fe/CoO interface, the state for which $\vec{S}_{CoO} \perp steps$ has a higher energy when $H \perp steps$ than when $H \parallel steps$, while the state for which $\vec{S}_{CoO} \parallel steps$ has a lower energy when $H \perp steps$ than

when $H \parallel steps$. Hence, the 90°-switching of the CoO spins from the state in which $\overleftrightarrow{S}_{CoO} \perp steps$ to the state in which $\overleftrightarrow{S}_{CoO} \parallel steps$ should encounter a lower energy barrier when $H \perp steps$ than when $H \parallel steps$, thus requiring a lower activation temperature.

The magnetic properties of the Fe/CoO bilayer could be strongly influenced by the CoO thickness. Therefore, a wedged sample was prepared consisting of a Fe(18 nm)/CoO(wedge) bilayer on a MgO(001) vicinal surface. Then the magnetic properties of Fe film were systematically measured by MOKE measurements after field cooling. Fig. 4 shows the phase diagrams of the hysteresis loop-shape as a function of the CoO thickness and the temperature, in which different measurement configurations are indicated by the inset in each graph. In Fig. 4(a) and 4(b), only two phases are observed when $H_{FC} \perp steps$. Phase I represents that the EA of the Fe film is parallel to the steps at high temperatures or thin CoO films, while phase II represents that the EA of the Fe film is perpendicular to the steps at low temperatures or thick CoO films. The CoO thickness of this SRT corresponds to the thickness at which the CoO AFM order is established. Due to the finite size effect, the T_N of the CoO film is expected to obey the following relation [36,37]:

$$\frac{T_N^b - T_N(d_{CoO})}{T_N^b} = \left(\frac{\xi_0}{d_{CoO}}\right)^{\lambda} \qquad (1)$$

Herein, T_N^b is the Néel temperature of the bulk film, ξ_0 is the magnetic correlation length at T = 0 K, and λ is the shift exponent for finite-size scaling. The boundary between the two phases in Fig. 4(a) and 4(b) can be well fitted by Eq. (1). The finite-size effect of the T_N of CoO has been studied in sputtered CoO/SiO_2 multilayers [36] and in ultrathin layers of CoO nanograins [37], and our results demonstrate that this is also valid for CoO epitaxial thin films.

When the sample was cooled down while $H_{FC} \parallel steps$, we observed an additional region (phase III), as shown in Fig. 4(c) and 4(d), which contains square EA loops

when $H \parallel steps$, and double-split HA loops when $H \perp steps$. Two SRTs can be found while increasing the temperature, as proven by the loops in Fig. 3(c) and 3(d). Moreover, we could observe three SRTs of Fe magnetization with different CoO thicknesses at low temperatures, which are further indicated by the typical hysteresis loops for different CoO thicknesses in Fig. 5. The boundaries between phases I and II in Fig. 4(c) and 4(d) can be attributed to the finite-size effect of the CoO ordering temperature, and can also be well-fitted by Eq. (1). For phase III, the EA of the Fe uniaxial anisotropy is, same for phase I, along the steps directions, but the uniaxial anisotropies of the Fe film in these two regions have different physical origins. Whereas the uniaxial anisotropy in phase I at high temperatures is induced by the atomic steps of the substrate with the paramagnetic CoO film, for phase III this anisotropy is induced by the spin-flop coupling between the Fe and CoO spins with $\vec{\vec{S}}_{CoO} \perp steps$.

It should be noted that phase III in Fig. 4(c) and 4(d) can only exist in a limited CoO thickness range. The upper boundary decreases with increasing temperature, while the lower boundary increases for higher temperatures. The lower boundary should be related to the 90°-switching of CoO AFM spins from $\vec{\vec{S}}_{CoO} \perp steps$ to $\vec{\vec{S}}_{CoO} \parallel steps$ due to thermal activation. The CoO spins should overcome the CoO four-fold volume anisotropy barrier while switching the spin orientation from the metastable state ($\vec{\vec{S}}_{CoO} \perp steps$) to the ground state ($\vec{\vec{S}}_{CoO} \parallel steps$). This energy barrier grows for increasing CoO thicknesses, thus requiring a larger thermal activation energy to overcome, thereby assuring that the transition thickness of the lower boundary increases with increasing temperature. The upper boundary should be related to the exchange coupling during the field-cooling process. In phase III, during the field-cooling process, the CoO AFM spins can overcome the step-induced AFM anisotropy owing to the spin-flop coupling, and remain in the metastable state with $\vec{\vec{S}}_{CoO} \perp steps$. The exchange coupling is usually an interfacial effect that is independent of the CoO thickness, and the step-induced anisotropy possibly increases

with increasing CoO thickness. Above a critical CoO thickness, the total step-induced AFM anisotropy could be larger than the spin-flop coupling energy. When this is the case, the CoO spins can not be influenced by the exchange coupling and stay along the easy axis parallel to the steps. Hence, for thick CoO films, only phase II can be observed. As indicated in Fig. 2(c), the exchange coupling strength between Fe and CoO decreases with increasing temperature. Therefore, the CoO SRT thickness between phase II and phase III also decreases for higher temperatures.

We attributed the SRT between phase I and II to the establishment of AFM order with in-plane uniaxial anisotropy and the spin-flop coupling. In FM/AFM single crystalline systems such as Fe/FeF_2 [38], Fe/stepped-Cr(001) [39], or Fe/MnPd [40], in-plane SRTs at temperatures close to the ordering temperature of the AFM layer have been observed experimentally. Fig. 2(c) and 2(d) clearly show that the SRT transition temperature is very close to the T_N of CoO film. In this case, the other possible origins of this SRT, such as the temperature-dependent strain induced AFM anisotropy change [31,41] and the crystallographic effect [42], can be excluded, since those effects should not be related to the establishment of the AFM order. As shown in Fig. 2(c), this SRT temperature is actually slightly lower than T_N, and this small temperature offset comes from the competition between the AFM anisotropy and the FM anisotropy. The AFM anisotropy energy should increase quickly with the decreasing temperature below T_N, and the interface exchange coupling drives the FM SRT once the AFM anisotropy energy is stronger than the FM anisotropy energy [43]. In Fe/NiO bilayers grown on vicinal Ag(001) [12], a second SRT was observed because of the EA switching of NiO AFM spins induced by the strain effect in the NiO film. Hence, in this case the NiO thickness of the second SRT is independent of the temperature. However, the lower temperature SRT induced by the thermally excited 90^o-switching of AFM spins in Fe/CoO bilayers has never been reported in the literature.

From the upper boundary between phase II and III, it is possible to estimate the strength of the step-induced AFM anisotropy. As shown in Fig. 2(c), the shift field Hs of the HA loop is 472 Oe at 80 K, and -23 Oe at 330 K with an EA switching of 90^o.

Typically, Hs can be used to estimate the uniaxial anisotropy of the FM layer by $K_u = H_s M d_{Fe}$ [32,33,34,44]. With this equation, the interfacial uniaxial anisotropy due to the spin-flop coupling is estimated to be 1.53 erg/cm^2 assuming a bulk Fe magnetization of M = 1714 emu/cm^3. When fixing Fe magnetization along the steps, the CoO spins will also feel this anisotropy energy difference between $\vec{S}_{CoO} \perp steps$ and $\vec{S}_{CoO} \parallel steps$. Since the upper boundary represents the balance condition between the step-induced anisotropy and the anisotropy induced by the spin-flop coupling in the CoO film, the area density of the step-induced AFM anisotropy in a 6.8-nm-thick CoO film at 80 K can be estimated to be ~ 1.53 erg/cm^2. Then the AFM uniaxial anisotropy can be approximated as 2.25×10^6 erg/cm^3. If assuming that the step-induced anisotropy only contains the volume contribution, this uniaxial anisotropy is one order of magnitude stronger than the anisotropy value for an Fe film [45], but is still much weaker than the magnetic anisotropy energy with the order of $10^8 erg/cm^3$ in bulk CoO AFM crystal [25, 46]. It should be noted that the step-induced uniaxial anisotropy in FM layers could either be located at the interface in Co/Cu systems [44] or extend into the bulk in Fe/Ag(001) systems [32]. The existence of the upper boundary of phase III in Fig. 4 indicates that thicker CoO films contain a larger step-induced AFM anisotropy. Therefore, the step-induced uniaxial anisotropy extends into the CoO film. Such step-induced AFM anisotropy should increase with the vicinal angle, which provides an effective way to continuously tune the AFM anisotropy.

IV. SUMMARY

In summary, we studied the magnetic properties of Fe/CoO bilayers grown on vicinal MgO(001) substrates. Using the XMLD technique, we found that the easy axis of the step-induced AFM anisotropy was aligned along the steps direction of the vicinal substrate, and the strength of the CoO uniaxial anisotropy was estimated to be 2.25×10^6 erg/cm^3. The effect of the step-induced CoO anisotropy on the exchange

coupling effect in Fe/CoO was studied by analyzing the SRT of Fe magnetization through MOKE measurements. For field cooling perpendicular to the steps direction, the easy axis of the Fe moment switches from perpendicular to parallel with respect to the steps direction around the T_N of CoO, whereas for field cooling parallel to steps direction, the system exhibits multiple SRTs, and the additional SRTs are attributed to the SRTs of AFM spins due to thermal activation. Our results show that the AFM spin orientation could be tuned with the ambient temperature, cooling field process and CoO thickness, and result in novel physical phenomena in FM/AFM systems.

ACKNOWLEDGMENTS

This work was supported by the National Key Basic Research Program (No. 2015CB921401, No. 2011CB921801) and the National Science Foundation (No. 11274074, No. 11434003, No. 11474066) of China.

FIGURE CAPTIONS

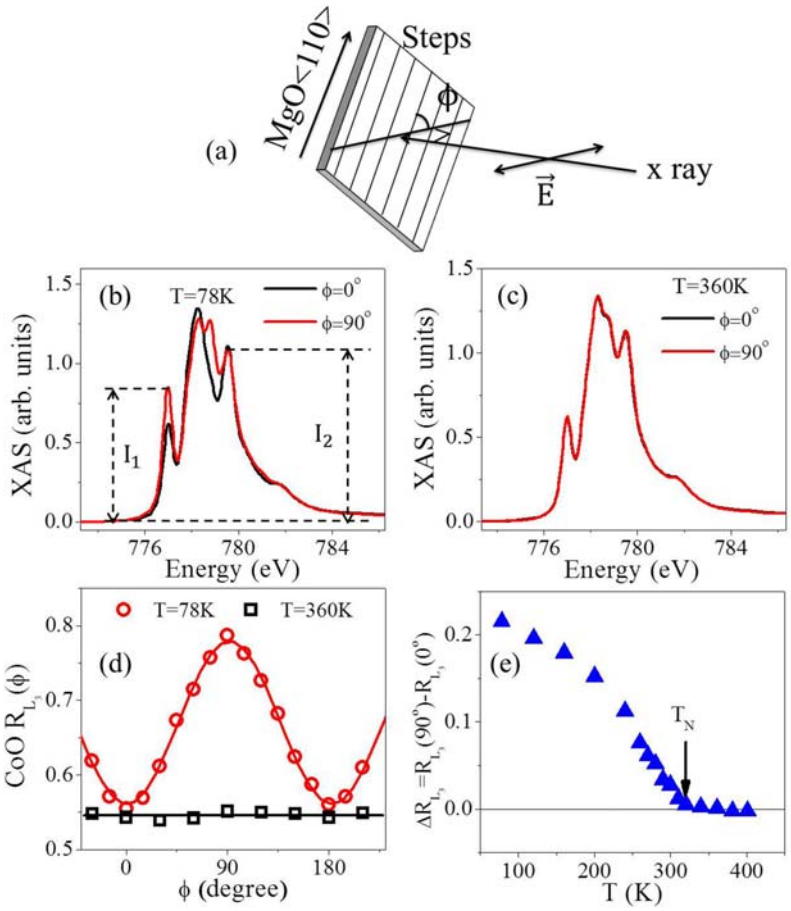

FIG. 1. (a) Schematic drawings of the XMLD measurement geometry. XAS spectra of the Co^{2+} L_3 edge at (b) T = 78 K and (c) T = 360 K for both $\phi = 0^o$ and $\phi = 90^o$ taken from a Au(2 nm)/CoO(6 nm)/vicinal MgO(001) system. (d) The CoO R_{L_3} as a function of ϕ for both T = 78 K and T = 360 K. The red continuous line represents a fitting curve using a cos(2ϕ) function, while the solid black line is a horizontal line that serves as a visual guide. (e) Temperature dependence of the L_3 ratio difference.

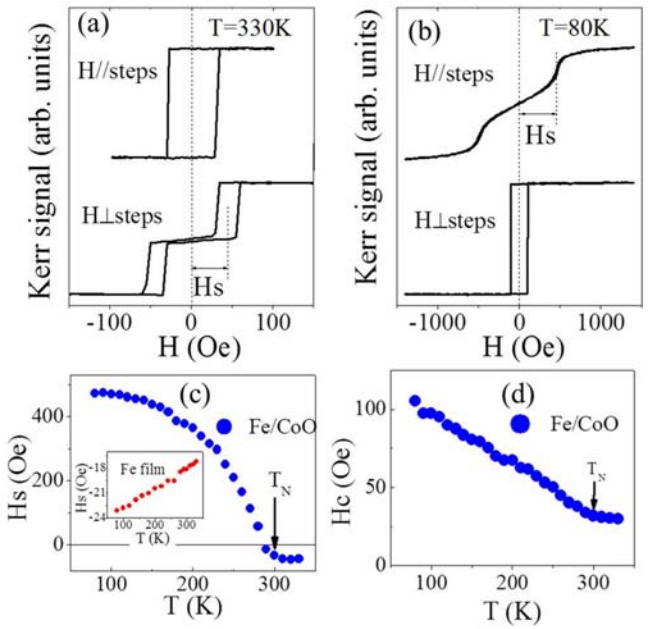

FIG. 2. Hysteresis loops of a Fe(18 nm)/CoO(4 nm) bilayer on a MgO(001) vicinal surface for $H \parallel steps$ and $H \perp steps$ at (a) T = 330 K and (b) T = 80 K after zero-field cooling. (c) Hs of HA loops and (d) Hc of EA loops as a function of the temperature. The inset in (c) shows the temperature-dependent Hs of an 18-nm-thick Fe film on the same MgO(001) vicinal surface.

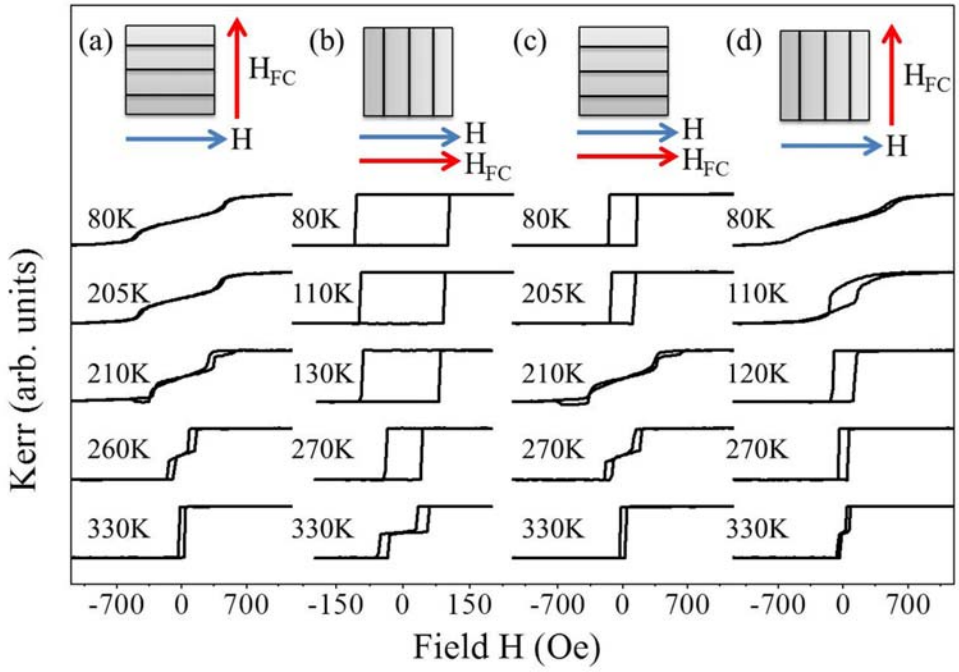

FIG. 3. Representative temperature-dependent hysteresis loops of a Fe(18 nm)/CoO(4 nm) bilayer on a MgO(001) vicinal surface for four different measurement geometries, being (a) $H_{FC} \perp steps$ and $H \parallel steps$, (b) $H_{FC} \perp steps$ and $H \perp steps$, (c) $H_{FC} \parallel steps$ and $H \parallel steps$, and (d) $H_{FC} \parallel steps$ and $H \perp steps$.

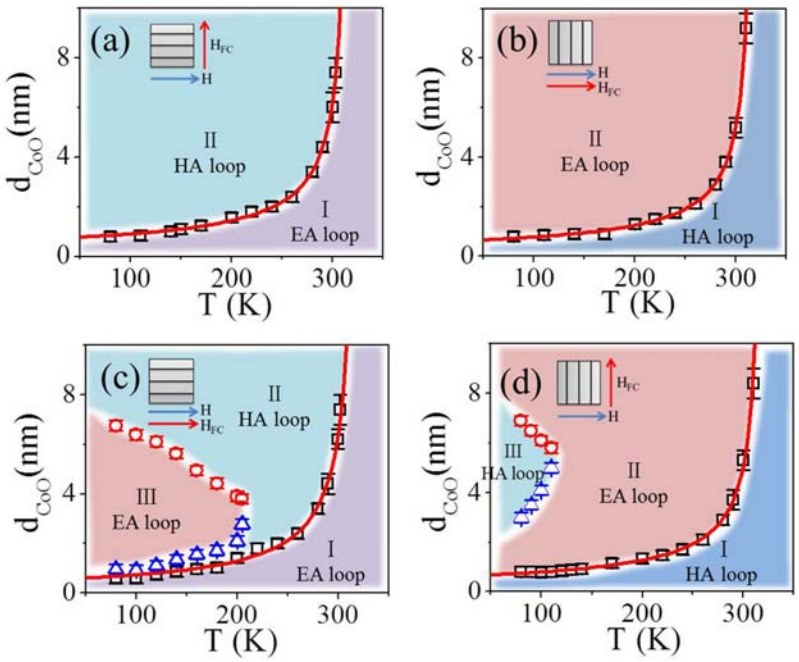

FIG. 4. Phase diagrams of the loop shapes as a function of the CoO thickness and the temperature for an Fe(18 nm)/CoO(0-12 nm) sample grown on MgO(001) vicinal surfaces. The measurement geometries are (a) $H_{FC} \perp steps$ and $H \parallel steps$, (b) $H_{FC} \perp steps$ and $H \perp steps$, (c) $H_{FC} \parallel steps$ and $H \parallel steps$, and (d) $H_{FC} \parallel steps$ and $H \perp steps$, as indicated by the inset in each graph. The red solid lines represent fitting results obtained using Eq. (1).

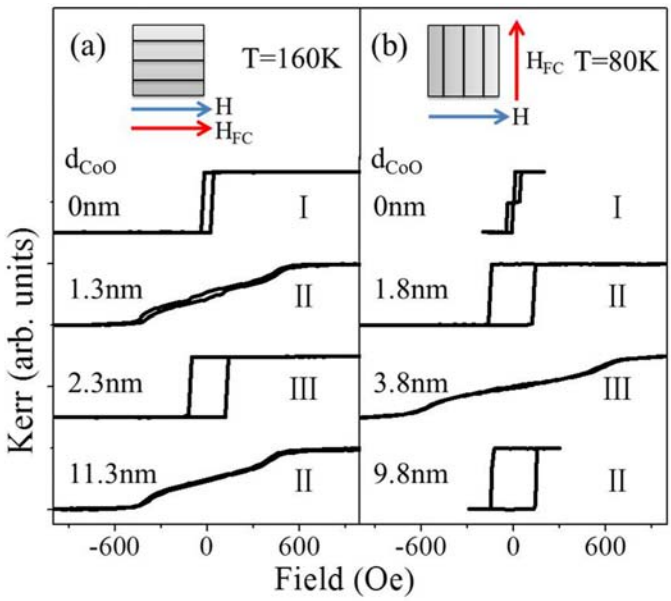

FIG. 5. Representative low-temperature hysteresis loops of Fe(18 nm)/CoO(d_{CoO}) samples with different CoO thicknesses after being cooled down with $H_{FC} \parallel steps$. (a) T = 160 K with $H \parallel steps$ and (b) T = 80 K with $H \perp steps$. The index numbers of the corresponding phases in Fig. 4 are marked next to the loops.

*wuyizheng@fudan.edu.cn

1 J. Nogues and I. K. Shuller, J. Magn. Magn. Mater. **192**, 203 (1999).

2 M. J. Kiwi, J. Magn. Magn. Mater. **234**, 584 (2001).

3 A. H. MacDonald and M. Tsoi, Phil. Trans. R. Soc. A **369**, 3098 (2011).

4 B. G. Park, J. Wunderlich, X. Martí, V. Holý, Y. Kurosaki, M. Yamada, H. Yamamoto, A. Nishide, J. Hayakawa, H. Takahashi, A. B. Shick, and T. Jungwirth, Nat. Mater. **10**, 347 (2011).

5 Y. Y. Wang, C. Song, B. Cui, G. Y. Wang, F. Zeng, and F. Pan, Phys. Rev. Lett. **109**, 137201 (2012).

6 Z. Wei, A. Sharma, A. S. Nunez, P. M. Haney, R. A. Duine, J. Bass, A. H. MacDonald, and M. Tsoi, Phys. Rev. Lett. **98**, 116603 (2007).

7 S. Urazhdin and N. Anthony, Phys. Rev. Lett. **99**, 046602 (2007).

8 X. Marti, I. Fina, C. Frontera, J. Liu, P. Wadley, Q. He, R. J. Paull, J. D. Clarkson, J. Kudrnovský, I. Turek, J. Kuneš, D. Yi, J-H. Chu, C. T. Nelson, L. You, E. Arenholz, S. Salahuddin, J. Fontcuberta, T. Jungwirth, and R. Ramesh, Nat. Mater. **13**, 367 (2014)

9 R. Ramesh and N. Spaldin, Nat. Mater. **6**, 21 (2007).

10 W. Kim, E. Jin, J. Wu, J. Park, E. Arenholz, A. Scholl, C. Hwang, and Z. Q. Qiu, Phys. Rev. B **81**, 174416 (2010).

11 S. I. Csiszar, M. W. Haverkort, Z. Hu, A. Tanaka, H. H. Hsieh, H.-J. Lin, C. T. Chen, T. Hibma, and L. H. Tjeng, Phys. Rev. Lett. **95**, 187205 (2005).

12 J. Li, E. Arenholz, Y. Meng, A. Tan, J. Park, E. Jin, H. Son, J. Wu, C. A. Jenkins, A. Scholl, H. W. Zhao, C. Hwang, and Z. Q. Qiu, Phys. Rev. B **84**, 012406 (2011).

13 J. Zhu, Q. Li, J. X. Li, Z. Ding, C. Y. Hua, M. J. Huang, H.-J. Lin, Z. Hu, C. Won, and Y. Z. Wu, J. Appl. Phys. **115**, 193903 (2014).

14 Y. Z. Wu, Z. Q. Qiu, Y. Zhao, A. T. Young, E. Arenholz, and B. Sinkovic, Phys. Rev. B **74**, 212402 (2006).

15 H. Matsuyama, C. Haginoya, and K. Koike, Phys. Rev. Lett. **85**, 646 (2000).

16 J. Li, M. Przybylski, F. Yildiz, X. L. Fu, and Y. Z. Wu, Phys. Rev. B **83**, 094436 (2011).

17 A. E. Berkowitz and K. Takano, J. Magn. Magn. Mater. **200**, 552 (1999).

18 M. D. Rechtin and B. L. Averbach, Phys. Rev. B **6**, 4294 (1972).

19 R. Abrudan, J. Miguel, M. Bernien, C. Tieg, M. Piantek, J. Kirschner, and W.

Kuch, Phys. Rev. B **77**, 014411 (2008).

20 E. Młyńczak, B. Matlak, A. Kozioł-Rachwał, J. Gurgu, N. Spiridis, and J. Korecki, Phys. Rev. B **88**, 085442 (2013).

21 J. Wu, J. S. Park, W. Kim, E. Arenholz, M. Liberati, A. Scholl, Y. Z. Wu, C. Hwang, and Z. Q. Qiu, Phys. Rev. Lett. **104**, 217204 (2010).

22 G. van der Laan, E. Arenholz, R. V. Chopdekar, and Y. Suzuki, Phys. Rev. B **77**, 064407 (2008).

23 W. L. Roth, Phys. Rev. **110**, 1333 (1958).

24 N. C. Koon, Phys. Rev. Lett. **78**, 4865 (1997).

25 T. C. Schulthess and W. H. Butler, Phys. Rev. Lett. **81**, 4516 (1998).

26 W. N. Cao, J. Li, G. Chen, J. Zhu, C. R. Hu, and Y. Z. Wu, Appl. Phys. Lett. **98**, 262506 (2011).

27 D. Alders, L. H. Tjeng, F. C. Voogt, T. Hibma, G. A. Sawatzky, C. T. Chen, J. Voge, M. Sacchi, and S. Iacobucci, Phys. Rev. B **57**, 11623 (1998).

28 M. W. Haverkort, S. I. Csiszar, Z. Hu, S. Altieri, A. Tanaka, H. H. Hsieh, H.-J. Lin, C. T. Chen, T. Hibma, and L. H. Tjeng, Phys. Rev. B **69**, 020408(R) (2004).

29 Y. Z. Wu, Y. Zhao, E. Arenholz, A. T. Young, B. Sinkovic, C.Won, and Z. Q. Qiu, Phys. Rev. B **78**, 064413 (2008).

30 H. Ohldag, A. Scholl, F. Nolting, S. Anders, F. U. Hillebrecht, and J. Stöhr, Phys. Rev. Lett. **86**, 2878 (2001).

31 H. Ohldag, G. van der Laan, and E. Arenholz, Phys. Rev. B **79**, 052403 (2009).

32 Y. Z. Wu, C. Won, and Z. Q. Qiu, Phys. Rev. B **65**, 184419 (2002).

33 W. Weber, A. Bischof, R. Allenspach, Ch. Würsch, C. H. Back, and D. Pescia, Phys. Rev. Lett. **76**, 3424 (1996).

34 Ch. Würsch, C. Stamm, S. Egger, D. Pescia, W. Baltensperger, and J. S. Helman, Nature **389**, 937 (1997).

35 N. J. Gökemeijer, R. L. Penn and D. R. Veblen and C. L. Chien, Phys. Rev. B **63**, 174422 (2001).

36 T. Ambrose and C. L. Chien, Phys. Rev. Lett. **76**, 1743 (1996).

37 M. Molina-Ruiz, A. F. Lopeandía, F. Pi, D. Givord, O. Bourgeois, and J. Rodríguez-Viejo, Phys. Rev. B **83**, 140407(R) (2011).

38 T. J. Moran, J. Nogués, D. Lederman, and I. K. Schuller, Appl. Phys. Lett. **72**, 617

(1998).

39 E. J. Escorcia-Aparicio, H. J. Choi, W. L. Ling, R. K. Kawakami, and Z. Q. Qiu, Phys. Rev. Lett. **81**, 2144 (1998).

40 Q.-F. Zhan and K. M. Krishnan, Appl. Phys. Lett. **96**, 112506 (2010).

41 S. Mandal and K. S. R. Menon, F. Maccherozzi and R. Belkhou, Phys. Rev. B **80**, 184408 (2009).

42 A. K. Suszka, O. Idigoras, E. Nikulina, A. Chuvilin, and A. Berger, Phys. Rev. Lett. **109**, 177205 (2012).

43 E. Jiménez, J. Camarero, J. Sort, J. Nogués, N. Mikuszeit, J. M. García-Martín, A. Hoffmann, B. Dieny, and R. Miranda, Phys. Rev. B **80**, 014415 (2009).

44 R. K. Kawakami, M. O. Bowen, H. J. Choi, E. J. Escorcia-Aparicio, and Z. Q. Qiu, Phys. Rev. B **58**, R5924 (1998).

45 G. Wastlbauer and J. A. C. Bland, Adv. Phys. **54**, 137 (2005).

46 A. Schrön, C. Rödl, and F. Bechstedt, Phys. Rev. B **86**, 115134 (2012).